By what mechanism is torus plasma heated (rather than adiabatically cooled) as it moves outward in the magnetosphere?

How are ions and electrons from the torus accelerated to form the extensive radiation belt?

How do relativistic electrons escape from Jupiter's magnetosphere with evidence of modulation at the Jovian spin period?

A comprehensive model of the Jovian magnetosphere should be expected not only to address these questions individually but also to expose the physical connections among the answers to these and many subsidiary questions. We have identified a number of conceptual ingredients that may be important in formulating such a model, and a number of problem areas where additional theoretical work is called for in the context of present observational knowledge. The development of a comprehensive model will, however, probably require a much broader data base than is available now. Only then will we be in a position to apply our understanding of Jupiter's magnetosphere with confidence to other magnetospheres outside the solar system.

ACKNOWLEDGMENTS

We are grateful to V. M. Vasyliunas, A. W. Schardt, F. Bagenal, D. F. Strobel, J. K. Alexander, R. A. Brown, F. C. Michel, D. L. Matson, J. F. Carbary, J. E. P. Connerney, J. A. Simpson, and R. E. Johnson for helpful comments. The work of TWH and AJD was supported in part by the National Science Foundation under grant ATM 80-19425 and the National Aeronautics and Space Administration under grants NAGW-166 and NAGW-168; the work of CKG was supported by the National Science Foundation under grant ATM76-82739 and the National Aeronautics and Space Administration under Contract NAS2-6553.

11
PLASMA DISTRIBUTION AND FLOW

Vytenis M. Vasyliunas

The highly extended magnetic field-line configuration of the Jovian magnetosphere with a near-equatorial current sheet and associated plasma sheet arises from mechanical stresses in the rotating plasma balanced by magnetic stresses. The relative geometrical thinness of the current sheet permits the use of several approximations in the description of the stress balance, each with a specified regime of validity in terms of taillike vs. dipolar field and hot vs. cold plasma; these include pressure balance, a simplified tangential stress balance, and an estimate of current-sheet thickness. A number of simple but quantitative models of the magnetic field are now available, including both theoretical models based on various assumptions about the distribution and degree of corotation of the plasma and empirical models intended to represent the observations. From the empirical models, values of plasma parameters required to maintain stress balance can be estimated. To obtain agreement between the estimated and the observed mass density values, it is necessary to assume that the azimuthal velocity of the plasma decreases significantly below rigid corotation in the outer magnetosphere. The uncertainties in the magnetic field component normal to the current sheet lead to sizable discrepancies among various estimates of the density or of the current sheet thickness. Azimuthal magnetic fields over the midnight-to-dawn quadrant are nearly independent of local time, in contrast to the situation in the terrestrial magnetosphere; they imply radial currents whose closure through the ionosphere is related to partial corotation. Generalization of Parker-spiral arguments to include a finite ionospheric conductivity provides a quantitative model for the azimuthal field. To keep the angular acceleration of the plasma within the required bounds, a mass flow of at least some 10^{30} to 10^{31} amu/s must be assumed but it is not yet clear whether this is a net outflow or primarily a circulation. Dipole tilt effects on the current sheet can be quantitatively modeled within the rigid corotation region; at larger distances, only qualitative propagating-wave descriptions plus empirical fits are available. Plasma flow models so far are mostly qualitative except for the description of partial corotation. The inability of magnetic stresses to maintain centripetal acceleration of a given flux tube content of plasma beyond a limiting distance is expected to result in a radial outflow (the planetary wind) and associated changes of magnetic field topology; the implied flow pattern is very similar qualitatively to the observed magnetospheric wind.

11.1. Introduction

The role of magnetospheric plasma in determining the configuration and dynamics of the magnetosphere is considerably more important at Jupiter than it is at Earth. If we imagine a sphere centered on the planet and require that the effects of the plasma inside the sphere on the magnetic field represent no more than a fractional perturbation of the total field, then the radius of the sphere could be allowed to reach almost the distance to the subsolar magnetopause at Earth but hardly a tenth of that at Jupiter. Consistency between the magnetic field configuration and the plasma distribution and flow is thus a major constraint on the physical description of almost the entire Jovian magnetosphere, whereas in the terrestrial case it is for most purposes a significant requirement only in the outermost boundary regions and the magnetotail. The main concern of this chapter is the extent to which various aspects of Jovian magnetospheric configuration and dynamics can be understood in a unified and self-consistent fashion

on the basis of present knowledge of the plasma population (Chaps. 3 and 4) and of the magnetic field (Chap. 1) together with appropriate theoretical models (Chap. 10). Most emphasis is placed here on the middle and outer magnetosphere, beyond the Io torus (the physics of the torus itself is discussed in Chaps. 3 and 6).

11.2. Plasma configuration in the middle and outer magnetosphere

1. Formulation of the problem

Beyond a distance of some 20 R_J from the planet, the Jovian magnetosphere contains highly distended magnetic field lines, with a near-equatorial current sheet and associated plasma sheet; the observational evidence for this configuration (which is a clear permanent feature of the observed predawn sector and is perhaps somewhat less clear on the dayside) is summarized in Chapters 1, 3, 4, 5, and 8. The physical description of such a stretched-out configuration requires considering stress balance both in a local and in a global context. Locally, there exists a magnetic force density that can be viewed either as arising from the Maxwell stress of the stretched-out field lines or, equivalently, as the $\mathbf{j} \times \mathbf{B}$ force of the magnetic field acting on the current sheet, balanced by mechanical plasma stresses to be identified and described. Globally, the large-scale pattern of the currents and the source of the mechanical stresses need to be considered.

A useful analog is provided by the tail of the terrestrial magnetosphere, which also contains a stretched-out field configuration with a current sheet and an associated plasma sheet. Locally, stress balance is maintained by counteracting the magnetic tension on the current sheet by a plasma pressure gradient in the direction along the magnetotail axis, by a similar gradient of plasma flow kinetic energy, by the tension resulting from a plasma pressure anisotropy, or by some combination of all three [see, e.g., Rich, Vasyliunas, and Wolf, 1972, for a detailed discussion]. The requirement of local stress balance strongly constrains the spatial variation of plasma and magnetic field properties; for example, in the two-dimensional approximation, detailed quantitative models of the plasma and field configuration can be constructed from suitable boundary conditions and the assumption that a plasma pressure gradient alone balances the magnetic stress [see, e.g., Schindler, 1975, 1979]. Globally, the stretched-out magnetotail configuration is the result of solar wind flow and specifically of the tangential stress exerted by the solar wind in its interaction with the magnetosphere. The power extracted by this tangential stress acting against solar wind flow represents the principal source of energy dissipated in the terrestrial magnetosphere [see, e.g., Siscoe and Cummings, 1970; Siscoe and Crooker, 1974; Akasofu, 1981].

The physical description of the middle and outer Jovian magnetosphere is in many ways similar to that of the terrestrial magnetotail, but with the difference that Jupiter's rotation rather than solar wind flow is generally thought to play the dominant role. Locally, the centripetal acceleration associated with any corotational motion of the plasma must be added to the list of possible contributors to stress balance. Globally, the stretched-out ('magnetodisc') configuration is considered to be the result of outward stresses ultimately derivable in some way from the planetary rotation. Unlike the case of a magnetotail formed by solar wind interaction, these stresses are predominantly perpendicular to the associated (corotational) flow and thus do not by themselves extract energy from the rotation; dissipation of rotational energy requires the additional presence of outward flow or azimuthal stress. Finally, one does expect that at

sufficiently large distances the importance of any rotational effects decreases and the solar wind becomes dominant in shaping the field-line configuration; it is, however, still a matter of debate where this transition occurs.

The quantitative formulation of local stress balance is contained in the momentum equation for the plasma

$$\rho(d\mathbf{V}/dt - \mathbf{g}) + \nabla \cdot \mathsf{P} = \mathbf{j} \times \mathbf{B} \tag{11.1}$$

together with two of Maxwell's equations

$$\nabla \times \mathbf{B} = \mu_0 \mathbf{j} \tag{11.2}$$

$$\nabla \cdot \mathbf{B} = 0 \tag{11.3}$$

In Equation (11.1), ρ is the mass density, $\mathbf{g}$ is the gravitational field (negligible for most purposes in the middle and outer magnetosphere),

$$d\mathbf{V}/dt = \partial\mathbf{V}/\partial t + \mathbf{V} \cdot \nabla\mathbf{V} \tag{11.4a}$$

is the acceleration of plasma bulk flow with respect to inertial space, and the rest of the symbols have their usual meaning. (In the rest of this chapter, the gravitational term will be omitted; it can always be reintroduced, if necessary, by the simple substitution $d\mathbf{V}/dt \rightarrow d\mathbf{V}/dt - \mathbf{g}$.) If the velocity $\mathbf{V}$ is referred not to inertial space but to a system of coordinates rotating with angular velocity ω, Equation (11.4a) is replaced by

$$\begin{aligned} d\mathbf{V}/dt = {} & \partial\mathbf{V}/\partial t + \mathbf{V} \cdot \nabla\mathbf{V} + \omega \times (\omega \times \mathbf{r}) \\ & + 2\omega \times \mathbf{V} - \mathbf{r} \times (\partial/\partial t + \mathbf{V} \cdot \nabla)\omega \end{aligned} \tag{11.4b}$$

where the added terms represent centrifugal, Coriolis, and (possible) differential rotation effects, respectively. The pressure tensor P should be well approximated by the gyrotropic form

$$\mathsf{P} = P_\perp \mathsf{I} + (P_\parallel - P_\perp)\,\mathbf{bb} \tag{11.5}$$

because the length scales of practically all magnetospheric structures of interest are large compared to typical particle cyclotron radii. It often proves convenient to eliminate $\mathbf{j}$ from Equation (11.1) by using (11.2) and (11.3) to write $\mathbf{j} \times \mathbf{B}$ in either of two equivalent forms:

$$\mu_0 \mathbf{j} \times \mathbf{B} = \mathbf{B} \cdot \nabla\mathbf{B} - 1/2\,\nabla B^2 \tag{11.6a}$$

$$= \nabla \cdot (\mathbf{BB} - 1/2\,B^2 \mathsf{I}) \tag{11.6b}$$

Equations (11.1)–(11.6) express the connection between the distribution of the plasma and the configuration of the magnetic field; at least in principle, they allow either one to be calculated from the other.

In applying these equations to construct models that might represent stress balance in the Jovian magnetosphere, several simplifications become possible. First, the observed magnetic field configuration indicates a well-defined and relatively thin current sheet; the length scales for spatial variations normal and transverse to the current sheet may be assumed to be of the order of, respectively, the sheet thickness h and the radial distance r, and hence the geometrical thin-sheet approximation $h << r$ may be consistently used. Second, most of the quantitative models developed to date are based on the physical assumption that the direction of the plasma bulk flow velocity is azimuthal, that is, corotational; this assumption, whose basis is discussed in Section 11.4.2, does not mean necessarily that other flow components are absent but merely that they are sufficiently small to have negligible direct dynamical effects. Third, axial symmetry

and time independence are often imposed as simplifying assumptions, neglecting any effects of dipole tilt relative to the rotation axis as well as any magnetic-anomaly effects; this makes the models more tractable mathematically but obviously restricts them to describing those aspects of the magnetosphere where tilt and anomaly effects are not important.

2. Implications of a thin current sheet

The thin-current-sheet approximation seems to be rather generally valid, and it is useful to consider its consequences for the stress balance equations before proceeding to more detailed (and more restricted) models. The approximation enables one (a) to derive an equation that describes directly the tangential stress on the current sheet, (b) to establish a pressure balance relation between the plasma and the magnetic field, and (c) to estimate the thickness of the current sheet and hence to check the validity of the assumed thin-sheet approximation.

For the quantitative description of local stress balance in the neighborhood of a point on the current sheet, introduce Cartesian coordinates with the z axis along the normal to the current sheet at that point, and let the subscript t denote (vector) quantities tangential to the current sheet; thus, for example, $\mathbf{B} = B_z\,\hat{\mathbf{z}} + \mathbf{B}_t$ and $\nabla = \hat{\mathbf{z}}\,\partial/\partial z + \nabla_t$. Maxwell's Equations (11.2) and (11.3) become

$$\mu_0\,\mathbf{j} = \hat{\mathbf{z}} \times (\partial \mathbf{B}_t/\partial t - \nabla_t B_z) + \nabla_t \times \mathbf{B}_t \tag{11.7}$$

$$0 = \partial B_z/\partial z + \nabla_t \cdot \mathbf{B}_t \tag{11.8}$$

The thin-sheet approximation is then expressed by the ordering

$$\partial/\partial z \sim O(1)/h \qquad \nabla_t \sim O(\epsilon)/h \tag{11.9}$$

where $\epsilon << 1$ is the ratio of current sheet thickness h to a gradient length scale in the tangential direction. It is convenient to define

$$\mathbf{B}_p \equiv \mu_0 \int dz\, \mathbf{j} \times \hat{\mathbf{z}} \tag{11.10}$$

which is equivalent to the relation

$$\mu_0\,\mathbf{j}_t = \hat{\mathbf{z}} \times \partial \mathbf{B}_p/\partial z \tag{11.11}$$

$\mathbf{B}_p$ may be thought of as the "planar" magnetic field associated with the local sheet current [cf., Mead and Beard, 1964] but it may also be viewed as simply a convenient representation of the current per unit length obtained by integrating the current density across either part of or the entire width of the current sheet. The advantage of introducing $\mathbf{B}_p$ is that it represents the only part of the magnetic field that varies on a spatial scale of current sheet thickness: with the magnetic field written as $\mathbf{B} = \mathbf{B}_p + (\mathbf{B} - \mathbf{B}_p)$, it is readily shown from (11.7), (11.8), and (11.11) that

$$(\partial/\partial z)\,(\mathbf{B} - \mathbf{B}_p) = \nabla_t B_z - \hat{\mathbf{z}}\,\nabla_t \cdot \mathbf{B}_t \tag{11.12}$$

If the current sheet is sufficiently thin, the quantity $\mathbf{B} - \mathbf{B}_p$ may be treated as constant, to within terms of $O(\epsilon)$, over its width. Note that

$$\mathbf{B}_t - \mathbf{B}_p = \int dz\, \nabla_t B_z \tag{11.13}$$

and thus $\mathbf{B}_p$ may be equated to $\mathbf{B}_t$, the tangential component of the entire field, again to $O(\epsilon)$ for a sufficiently thin sheet. The Lorentz force density may be written as

$$\mu_0\,\mathbf{j} \times \mathbf{B} = -\hat{\mathbf{z}}\,\mathbf{B}_p \cdot \partial \mathbf{B}_p/\partial z + \mu_0\,\mathbf{j}_t \times (\mathbf{B} - \mathbf{B}_p) + (\nabla_t \times \mathbf{B}_t) \times \mathbf{B}_t \tag{11.14}$$

This expression is exact; the thin-sheet approximation consists in neglecting the last term (associated with an obviously small z component of $\mathbf{j}$ due, for example, to an azimuthally varying width of the current sheet) and in treating $\mathbf{B} - \mathbf{B}_p$ in the second term as independent of z.

Tangential stress balance. The components of the momentum Equation (11.1) tangential to the current sheet may now be written as

(11.15)

$$\rho(d\mathbf{V}/dt)_t + \nabla_t P_\perp + \nabla_t \cdot (P_\parallel - P_\perp)\,\mathbf{b}_t\,\mathbf{b}_t + (\partial/\partial z)\,(P_\parallel - P_\perp)\,b_z\,\mathbf{b}_t = (1/\mu_0)\,B_z\,\partial \mathbf{B}_p/\partial z$$

where Equations (11.5), (11.14) with the previously mentioned thin-sheet approximations, (11.11), and the fact that $\hat{\mathbf{z}} \cdot (\mathbf{B} - \mathbf{B}_p) = B_z$ have been used; $(d\mathbf{V}/dt)_t$ is of course the tangential part of the acceleration (to be distinguished from the time derivative of the tangential velocity!). Equation (11.15) balances the tangential components of inertial stress and pressure gradient (first two terms on the LH side) against the tension of magnetic field lines crossing the current sheet (RH side), with both the pressure gradient and the magnetic tension modified by additional terms dependent on pressure anisotropy (last two terms on the LH side). If the plasma flow is predominantly azimuthal,

$$\mathbf{V} = \omega \times \mathbf{r} \tag{11.16}$$

where ω may or may not be equal to Ω_J (see Sec. 11.D.2), then the acceleration is

$$d\mathbf{V}/dt = \omega \times (\omega \times \mathbf{r}) = -\omega^2\,(\mathbf{r} - \hat{\omega}\mathbf{r} \cdot \hat{\omega}) \equiv -\omega^2\,\mathbf{R} \tag{11.17}$$

and points inward toward the rotation axis; the pressure normally decreases with increasing radial distance in the outer magnetosphere and hence the pressure gradient also points inward. The magnetic tension is thus required to point inward, which it does as long as the signs of $\mathbf{B}_p$ (or $\mathbf{B}_t$) and B_z are those appropriate to stretched-out but closed field lines from the planet.

Two variants of Equation (11.15) are of interest for further developments. On the field reversal surface, defined by the condition $\mathbf{B}_t = 0$, (11.15) can be cast into the rather simple form

$$\rho(d\mathbf{V}/dt)_t + \nabla_t P_\perp + (P_\parallel - P_\perp)\,\nabla_t B_z/B_z = (B_z\,\xi/\mu_0)\,\partial \mathbf{B}_p/\partial z \tag{11.18}$$

where $\xi \equiv 1 - \mu_0(P_\parallel - P_\perp)/B^2$ (note that $B = B_z$ on the field reversal surface). Equation (11.18) is actually exact (for the case $\mathbf{B}_t = 0$), with no thin-sheet approximations. One may also integrate (11.15) across the full width of the current sheet to obtain the equation for the tangential force per unit area:

$$\sigma(d\mathbf{V}/dt)_t + \nabla_t \int dz\, P_\perp + \nabla_t \cdot \int dz\,(P_\parallel - P_\perp)\,\mathbf{b}_t\,\mathbf{b}_t = (1/\mu_0)B_z\,[\mathbf{B}_p] \tag{11.19}$$

Here $\sigma \equiv \int dz\,\rho$ is the mass density per unit area, and $[\mathbf{B}_p]$ is the vector difference of $\mathbf{B}_p$ above and below the current sheet; from Equation (11.10),

$$[\mathbf{B}_p] = \mu_0\,\mathbf{j}' \times \hat{\mathbf{z}} \tag{11.20}$$

with $\mathbf{j}'$ the sheet current density per unit length. To obtain Equation (11.19) several thin-sheet approximations have been used, in particular constancy of B_z and of $(d\mathbf{V}/dt)_t$ over the sheet thickness and neglect of $P_\parallel - P_\perp$ compared to B^2/μ_0 outside the sheet. Furthermore, if the current sheet is sufficiently thin in the sense that its thickness is allowed to become small while σ and P are held fixed, the pressure terms in (11.19) may be dropped.

Pressure balance. The component of the momentum Equation (11.1) normal to the current sheet may be written, after some manipulation of (11.14), as

$$\rho(d\mathbf{V}/dt)\cdot\hat{\mathbf{z}} + \partial P_{zz}/\partial z + \nabla_t\cdot(P_\parallel - P_\perp)\mathbf{b}_t b_z \tag{11.21}$$

$$= -(1/\mu_0)\left[\frac{\partial}{\partial z}\left(\frac{1}{2}B_p^2\right) + (\mathbf{B}-\mathbf{B}_p)\cdot\partial\mathbf{B}_p/\partial z\right]$$

The third term on the LH side is quite generally $O(\epsilon)$ compared to the second and vanishes entirely if the plasma pressure is isotropic. On the RH side, the thin-sheet approximation of $\mathbf{B}-\mathbf{B}_p$ independent of z may be invoked. Equation (11.21) may then be rewritten

$$\frac{\partial}{\partial z}\left[P_{zz} + B_p^2/2\mu_0 + \mathbf{B}_p\cdot(\mathbf{B}-\mathbf{B}_p)/\mu_0 + \int^z dz'\,\rho(d\mathbf{V}/dt)\cdot\hat{\mathbf{z}}\right] = 0 \tag{11.22}$$

which, when integrated with respect to z, states that the quantity in brackets remains constant across the width of the current sheet [more precisely, undergoes a fractional variation of no more than $O(\epsilon)$]. The magnetic terms in (11.22), which may be rewritten as

$$(1/2)B_p^2 + \mathbf{B}_p\cdot(\mathbf{B}-\mathbf{B}_p) = (1/2)B_t^2 - (1/2)|\mathbf{B}_t-\mathbf{B}_p|^2 \tag{11.23}$$

represent the pressure of the tangential magnetic field (minus the pressure of its curl-free part $\mathbf{B}_t-\mathbf{B}_p$ if it is not negligible). Thus, Equation (11.22) is the familiar statement of pressure balance between the plasma and the magnetic field modified by an added term representing the inertial stress of acceleration normal to the sheet. If the plasma pressure is isotropic, P_{zz} is simply the pressure P; otherwise, from Equation (11.5),

$$P_{zz} = P_\parallel b_z^2 + P_\perp(1-b_z^2). \tag{11.24}$$

Note in particular that $P_{zz} = P_\parallel$ at the field reversal surface where $\mathbf{B}_t = 0$. (Note also that the thermal energy density of the plasma is always $(1/2)(P_{xx}+P_{yy}+P_{zz}) = (1/2)P_\parallel + P_\perp$, which is not equal to P_{zz} except in the singular case when $2P_\perp/P_\parallel = 1-(B_t/B_z)^2$; the balancing of plasma and magnetic energy densities instead of pressures, as in Walker, Kivelson, and Schardt [1978] or Lanzerotti et al. [1980], is incorrect, being in error by a factor of 3/2.)

Thickness of the current sheet. We may now obtain an order-of-magnitude estimate for h, starting with the approximate definition

$$\frac{1}{h} \simeq \frac{1}{B_p^*}\left|\frac{\partial}{\partial z}\mathbf{B}_p\right| \tag{11.25}$$

where $\partial\mathbf{B}_p/\partial z$ is to be evaluated at the field reversal surface from the tangential stress balance relation (11.18) and $2B_p^* = |[\mathbf{B}_p]|$, the magnitude of the vector change of $\mathbf{B}_p$ across the entire width of the current sheet (the factor 2 makes $B_p^* = |\mathbf{B}_p|$ on either side of the current sheet for the symmetric case and means that h is actually the halfwidth). It is apparent from Equations (11.11) and (11.10) or (11.20) that this estimate gives the thickness as the ratio of current per unit length to the current density at a representative location within the current sheet. A specific model for the mechanical stresses on the LH side of (11.18) must be adopted. Following common practice, we assume the acceleration to be that associated with azimuthal flow [Eqs. (11.16) and (11.17)] with speed $V_\phi = \omega r$ and the gradients of the pressure and the magnetic field to be radial; we write

$$\nu \equiv -\partial\log P_\perp/\partial\log r \qquad \nu_z \equiv -(1/B_z)\,\partial B_z/\partial\log r \tag{11.26}$$

and define the thermal speeds $w_\perp$, $w_\parallel$ by

$$P_\perp \equiv \rho w_\perp^2 \qquad P_\parallel \equiv \rho w_\parallel^2 \tag{11.27}$$

Combining (11.25)–(11.27) with (11.18) yields an estimate for h

$$\frac{h}{r} \simeq \left|\frac{B_p^*}{B_z}\right| \frac{(B_z^2/\mu_0\rho) + w_\perp^2 - w_\parallel^2}{V_\phi^2 + \nu w_\perp^2 + \nu_z(w_\parallel^2 - w_\perp^2)} \tag{11.28}$$

where all the quantities on the RH side (with the exception of B_p^*) are to be evaluated at the field reversal surface. It is convenient to rewrite (11.28) in the form

$$\frac{h}{r} \simeq \left|\frac{B_p^*}{B_z}\right| \frac{[B_z^2/\mu_0\rho(V_\phi^2 + \nu w_\perp^2)]\,(1-\chi)}{1 + \nu_z\chi[B_z^2/\mu_0\rho(V_\phi + \nu w_\perp^2)]} \tag{11.29}$$

where

$$\chi \equiv \mu_0\rho(w_\parallel^2 - w_\perp^2)/B_z^2 \tag{11.30}$$

On physical grounds one expects $|\chi| < 1$ (if $|\chi| \gtrsim 1$, the plasma will be subject to either the firehose or the mirror instability, depending on the sign of χ), and Equation (11.29) then makes it apparent that the order of magnitude of h/r is not greatly affected by plasma pressure anisotropies as long as these are no larger than what is plausible.

The main question about the thickness is not whether it is small in the merely geometrical sense $h << r$ but whether it is small enough to ensure the validity of the various results derived from the thin-sheet approximation, which are principally the following:

(1) Pressure balance, Equation (11.22). The crucial step in the derivation was the neglect of the term $\mathbf{B}_p\cdot(\partial/\partial z)(\mathbf{B}-\mathbf{B}_p)$ compared to $(\partial/\partial z)B_p^2/2$; with $(\partial/\partial z)(\mathbf{B}-\mathbf{B}_p)$ given by (11.12) and $\partial B_p/\partial z$ approximated by B_p^*/h, the criterion for its validity is readily shown to be

$$\nu_z\left|\frac{B_z}{B_p^*}\right|\frac{h}{r} << 1 \tag{11.31}$$

(2) The near equality $\mathbf{B}_p \approx \mathbf{B}_t$. From Equation (11.13) we obtain

$$\mathbf{B}_t - \mathbf{B}_p \sim h\,\nabla_t B_z \sim -\nu_z B_z h/r \tag{11.32}$$

so that the criterion for $|\mathbf{B}_t-\mathbf{B}_p| << B_p^*$ is the same as (11.31).

(3) Constancy of B_z across the thickness of the current sheet, used in deriving the tangential force Equation (11.19). The change of B_z is given by the integral of (11.8) as

$$\delta B_z = -\int dz\,\nabla_t\cdot\mathbf{B}_t \sim \nu_r B_t h/r \tag{11.33}$$

where ν_r, analogously to ν_z, is a measure of the radial gradient of B_t. Taking into account the relation between $\mathbf{B}_t$ and $\mathbf{B}_p$ given by (11.32), with due regard to signs, we obtain as the criterion for $|\delta B_z/B_z| << 1$

$$\nu_r\left[\frac{h}{r}\left|\frac{B_p^*}{B_z}\right| + \nu_z\left(\frac{h}{r}\right)^2\right] << 1 \tag{11.34}$$

(4) Localization of field lines crossing the current sheet. The radius vector to a point on a magnetic field line undergoes, across a half-thickness of the current sheet, a tangential change given by

$$\delta \mathbf{r}_t = \int dz\, \mathbf{B}_t / B_z \sim h B_t / B_z \tag{11.35}$$

where the integration in this case follows the field line; however, if $|\delta \mathbf{r}_t| << r$, integrals along the field line may be equated to simple integrals across the width of the current sheet at a fixed location. Comparison of (11.35) with (11.33) shows that the criterion for $|\delta \mathbf{r}_t / r| << 1$ is the same as that for $|\delta B_z / B_z| << 1$ and hence given by (11.34), except for absence of the factor ν_r.

There are thus two distinct thin-sheet approximations, embodied in conditions (11.31) and (11.34), respectively. The first implies pressure balance and the identification $\mathbf{B}_p \sim \mathbf{B}_t$; then $B_p{}^*$ can be determined either from observations of the actual magnetic field just outside the current sheet or by applying the pressure balance relation (11.22) between the field reversal surface and the outside with the result

$$B_p{}^{*2} \simeq 2\mu_0 \rho w_\parallel{}^2 \tag{11.36}$$

(the inertial terms have here been neglected, as their normal component is usually relatively small). To satisfy the inequality in (11.31) it is sufficient and (if we ignore the improbable singular case $\chi \simeq 1$) necessary to have

$$B_z{}^2 / \mu_0 \rho (V_\phi{}^2 + \nu w_\perp{}^2) << 1 \tag{11.37}$$

which can be rewritten, since (11.36) holds if the inequality does, as

$$(B_z / B_p{}^*)^2 [2 w_\parallel{}^2 / (V_\phi{}^2 + \nu w_\perp{}^2)] << 1 \tag{11.38}$$

With a limit on the plasma pressure anisotropy set by

$$\frac{w_\parallel{}^2 - w_\perp{}^2}{w_\parallel{}^2} = \chi \frac{B_z{}^2}{\mu_0 \rho w_\parallel{}^2} = 2\chi \left(\frac{B_z}{B_p{}^*} \right)^2 \tag{11.39}$$

with $|\chi| < 1$, it is readily shown that in the case $|B_z| << |B_p{}^*|$ (which we call a *taillike* field) the inequality (11.38) and hence (11.31) is automatically satisfied without any additional assumptions [a result that can also be seen directly from (11.31) if we recall that h/r should in no case be larger than $O(1)$], whereas in the case of a nontaillike or nearly dipolar field $|B_z| \gtrsim |B_p{}^*|$ or $|B_z| >> |B_p{}^*|$ the inequality requires $V_\phi{}^2 >> \omega_\perp{}^2$ and $V_\phi{}^2 >> \omega_\parallel{}^2$ as well as $B_z{}^2 / \mu_0 \rho V_\phi{}^2 << 1$. Pressure balance, therefore: (a) always holds, whether the plasma be cold or hot, in the case of a highly stretched-out, taillike field configuration, such as is found in the outer regions of the Jovian magnetosphere; (b) in the nearly dipolar field of the inner regions, holds only if the plasma is sufficiently cold, that is, the azimuthal flow speed V_ϕ exceeds the thermal speed, and if furthermore V_ϕ appreciably exceeds the Alfvén speed in the current sheet; (c) does not hold in a strongly dipolar field defined by the condition $B_z{}^2 \gtrsim \mu_0 \rho V_\phi{}^2$. Whenever pressure balance does hold, it is convenient for most purposes to express the thickness of the current sheet as

$$\frac{h}{r} = \left| \frac{B_z}{B_p{}^*} \right| \frac{2 w_\parallel{}^2 (1 - \chi)}{V_\phi{}^2 + \nu w_\perp{}^2} \tag{11.40}$$

obtained from (11.29) by using (11.36) to eliminate ρ and (11.37) to drop small terms. Equation (11.40) is the basis for most observational models of current sheet thickness to be discussed in Section 11.3.3.

Table 11.1. *Validity of thin-sheet approximations*

	Plasma:	Pressure balance, $\mathbf{B}_p = \mathbf{B}_t$		B_z = constant, $(\delta \mathbf{r}_t)_{\text{field line}} << r$	
		Hot	Cold	Hot	Cold
Magnetic field:					
$B_p{}^* >> B_z$	Tail-like	Yes	Yes	No	Yes
$B_p{}^* \lesssim B_z$ or $B_p{}^* << B_z$ $B_z{}^2 << \mu_0 \rho V_\phi{}^2$	Nearly dipolar	No	Yes	No	Yes
$B_z{}^2 \gtrsim \mu_0 \rho V_\phi{}^2$	Strongly dipolar	No	No	No	Yes

The other thin-sheet approximation, given by inequality (11.34), implies constancy of B_z and negligible change of tangential location of a field line across the thickness of the current sheet; an important corollary is that the plasma content of a flux tube per unit magnetic flux, defined by an integral along the field line as

$$\eta \equiv \int d\ell\, \frac{\rho}{B} \tag{11.41}$$

can then be simply approximated as

$$\eta = \int d\ell\, \frac{\rho}{B} = \int dz\, \frac{\rho}{B_z} \simeq \frac{\sigma}{B_z} \tag{11.42}$$

The condition $h/r << 1$ is evidently necessary for (11.34) to hold; in the case $|B_z| \gtrsim |B_p{}^*|$ or $|B_z| >> |B_p{}^*|$ it is also sufficient, but in this same case $h/r << 1$ is implied by pressure balance [cf., Eq. (11.29) and inequality (11.37)]. Thus, for a nearly dipolar field, the constant B_z approximation holds under the same conditions when pressure balance does, that is, when the plasma is cold. It will shortly be shown that for a strong dipolar field the constant B_z approximation also holds when the plasma is cold. Finally, for a taillike field, substituting h/r from (11.40) and using the fact that [Eq. (11.39)] $w_\perp{}^2 \simeq w_\parallel{}^2 = w^2$ to within $O(B_z / B_p{}^*)^2$ we reduce (11.34) to the approximate form

$$\frac{2\nu_r w^2}{V_\phi{}^2 + \nu w^2} << 1 \tag{11.43}$$

in which the inequality is satisfied if and only if $V_\phi{}^2 >> w^2$. Thus, quite generally, the constant B_z approximation holds only when the plasma is cold; the presure gradient terms in the tangential force Equation (11.19) should be neglected whenever constancy of B_z has been invoked. (Statements by Gleeson and Axford [1976] and by Goertz [1976b] that B_z = constant follows merely from $h/r << 1$ are thus not correct, although the calculation of Gleeson and Axford is self-consistent inasmuch as they drop the tangential pressure gradients, whereas Goertz does not.)

Table 11.1 summarizes the results on the validity of both the thin-sheet approximations under various magnetic field and plasma conditions.

Although the method described so far for estimating the thickness of the current sheet is in principle valid generally, in practice it does not provide useful estimates of h/r when pressure balance does not hold, since there is then no ready way of evaluating B_p^* in Equation (11.28) or (11.29): one can neither calculate B_p^* from the pressure balance relation nor equate it to the measured tangential component of the field. However, an alternative approach to estimating the thickness may be taken. The component of the momentum Equation (11.1) parallel to the magnetic field may be written, with a gyrotropic pressure tensor (11.5) and after some manipulation,

$$\rho \left(\frac{d\mathbf{V}}{dt} \right) + \frac{\partial}{\partial \ell} P_\parallel - (P_\parallel - P_\perp) \frac{\partial}{\partial \ell} \log B = 0 \tag{11.44}$$

where $\partial/\partial\ell \equiv \hat{\mathbf{b}} \cdot \nabla$ and the RH side is of course zero since $\mathbf{j} \times \mathbf{B}$ has no parallel component. The parallel component of the acceleration, with the usual assumption of azimuthal flow, may be written

$$\left(\frac{d\mathbf{V}}{dt} \right)_\parallel = -\omega^2 \mathbf{R} \cdot \hat{\mathbf{b}} = -\frac{\partial}{\partial \ell} \left(\frac{1}{2} \omega^2 R^2 \right) \tag{11.45}$$

where $\mathbf{R}$ is the cylindrical radial distance from the rotation axis [cf., Eq. (11.17)] and the constancy of ω along a field line, implied by Ferraro's isorotation theorem, has been used. Equation (11.44) may be considered an equation for the variation of $P_\parallel$ along a field line:

$$\frac{\partial}{\partial \ell} \log P_\parallel = \frac{\rho}{P_\parallel} \frac{\partial}{\partial \ell} \left(\frac{1}{2} \omega^2 R^2 \right) + \left(1 - \frac{P_\perp}{P_\parallel} \right) \frac{\partial}{\partial \ell} \log B \tag{11.46}$$

Given the necessary assumptions about the pressure-density relation and the magnetic field geometry, Equation (11.46) can be integrated to obtain the profile of ρ along the field line and hence the thickness h; note that the thickness now refers, in the first instance, to the plasma sheet (as distinct from the current sheet). This approach is in practice useful primarily in regions of strong dipolar field where $\mathbf{B}_p$ is a small perturbation of the total field $\mathbf{B}$, so that the field geometry is approximately known independently of the current sheet (whereas in regions of taillike field the geometry is strongly influenced by the current sheet itself and cannot be specified without already knowing the sheet thickness); its range of applicability thus neatly complements that of the previously described approach based on stress balance.

An important special case is that of isotropic pressure, when (11.46) reduces to

$$\frac{\partial}{\partial \ell} \log P = \frac{\rho}{P} \frac{\partial}{\partial \ell} \left(\frac{1}{2} \omega^2 R^2 \right) \tag{11.47}$$

(Note that Eq. (11.47) implies, with no additional assumptions, that the maximum pressure on any given field line is found at the point where the field line reaches its greatest distance R_0 from the rotation axis, or equivalently where $\mathbf{B} \cdot \mathbf{R} = 0$, a fact of significance for the discussion of dipole tilt effects in Sec. 11.3.5.) With the further assumption of isothermal behavior, $P/\rho = w^2$ constant along a given field line, Equation (11.47) can be explicitly integrated to yield

$$\rho = \rho_0 \exp \left\{ -\frac{1}{2} \frac{\omega^2}{w^2} (R_0^2 - R^2) \right\} \tag{11.48}$$

To relate $R_0^2 - R^2$ to the distance z from the center of the sheet a model for the magnetic field lines must be adopted. For a dipolar field one obtains

$$R_0^2 - R^2 = 3z^2 \tag{11.49}$$

to lowest order in $(z/R_0)^2$; the factor 3 is the ratio of field-line radius of curvature to radial distance near the equator [cf., e.g., Roederer, 1970, pp. 53, 58]. Equation (11.48) then represents a Gaussian profile

$$\rho = \rho_0 \exp \left\{ -\frac{3}{2} \frac{\omega^2 z^2}{w^2} \right\} \tag{11.50}$$

and the plasma sheet thickness is given by the width of the Gaussian as

$$\frac{h}{r} \simeq \left(\frac{2}{3} \right)^{1/2} \frac{w}{\omega r} = \left(\frac{2}{3} \right)^{1/2} \frac{w}{V_\phi} \tag{11.51}$$

whence follows the previously stated conclusion that $h/r << 1$ in a strongly dipolar field if the plasma is cold. The results (11.50) and (11.51) are well known in the literature, for example, Hill and Michel [1976], Siscoe [1977]; h given by (11.51) is sometimes called the centrifugal scale height.

Explicit density profiles can be derived by integration of (11.46) in a few other cases. If adiabatic behavior is assumed, P/ρ^γ = constant, one obtains

$$\rho = \rho_0 \left\{ 1 - \frac{\gamma - 1}{2\gamma} \frac{\omega^2}{w_0^2} (R_0^2 - R^2) \right\}^{\frac{1}{\gamma - 1}} \tag{11.52}$$

where w_0 is the thermal speed at the center of the sheet; this result, which of course reduces to (11.48) as $\gamma \to 1$, was discussed by Mendis and Axford [1974] in the somewhat different context of an ionospheric plasma source. Assumption of the Chew-Goldberger-Low (CGL) double adiabatic relations

$$P_\perp/\rho B = \text{constant} \quad P_\parallel B^2/\rho^3 = \text{constant} \tag{11.53}$$

[e.g., Rossi and Olbert, 1970, p. 358] can be shown to give

$$\rho = \rho_0 \frac{B}{B_0} \left\{ 1 - \frac{\omega^2}{3w_\parallel^2} (R_0^2 - R^2) - \frac{2}{3} \left(\frac{w_\perp}{w_\parallel} \right)^2 \left(\frac{B}{B_0} - 1 \right) \right\}^{1/2} \tag{11.54}$$

where $w_\parallel$ and $w_\perp$ represent values at the center of the sheet, although the subscript 0 has been omitted for ease of reading; with the use of (11.49) and a corresponding near-equatorial approximation for B/B_0, (11.54) becomes, to lowest order in $(z/R_0)^2$,

$$\rho \simeq \rho_0 \left\{ 1 - \frac{z^2}{r^2} \frac{V_\phi^2 + 3w_\perp^2}{w_\parallel^2} \right\}^{1/2} \tag{11.55}$$

However, the results (11.52) and (11.54) are mainly of academic interest because the assumed equation of state — either adiabatic or CGL — holds, if at all, along a plasma flow line; there is no reason to expect either one to hold along a magnetic field line, unless the plasma flow were indeed predominantly field aligned.

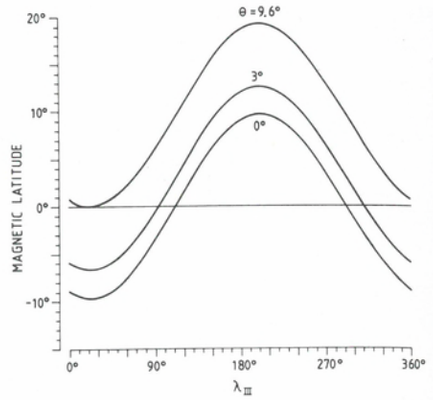

Fig. 11.1. Dipole magnetic latitude as a function of System III longitude for a spacecraft at a fixed angle θ above the rotational equator [from Vasyliunas and Dessler, 1981]. The bulk of available observations in the outer Jovian magnetosphere lie between $\theta = 3°$ and $\theta = 5°$ (Voyager 1 and 2) and near $\theta \approx 9°$ (Pioneer 10), plus the high-latitude pass ($\theta \approx 30°$) of Pioneer 11 outbound near the local noon. Note the absence of coverage near the magnetic equator for the longitude range 120°–300°, which includes the active sector.

11.3. Models of the magnetic field and stress balance

After the preceding survey of general principles and approximations, we turn to a discussion of specific models for the magnetic field in the middle and outer Jovian magnetosphere. Chapter 1 discusses the purely magnetic aspects of many of the models, their relation to observations of the field, and the complex and longitudinally asymmetric nondipolar internal magnetic field that provides the basis for the magnetic anomaly model (see Chap. 10) but otherwise has no significant direct effects at distances beyond a few R_J; in this chapter, we are concerned with the relation of the magnetic field to stress balance, the implications for the distribution of plasma, and the agreement (or otherwise) with observed plasma properties.

The models may be grouped into two classes, conveniently labeled theoretical and empirical, respectively, although a more fundamental distinction is whether the magnetic field is calculated from the plasma distribution or vice versa. Theoretical models as a rule start with assumptions about the plasma and thence derive the configuration of the magnetic field; empirical models are to a greater or lesser extent constructed as representations of the observed magnetic field and serve as a basis for inferences about properties of the plasma.

Axial symmetry plays a role, explicitly or implicitly, in most existing models. Theoretical models generally assume no dependence either on local time or on longitude (thereby necessarily treating the planetary magnetic dipole moment as aligned with the rotation axis). Empirical models are often derived from observations over a limited range of local times and thus nominally require no global assumptions about local time dependence (although derivatives with respect to local time over that limited range are as a rule set to zero or ignored), but neglect of any dependence on Jovian longitude other than the geometrical effects of dipole tilt (see Sec. 11.3.5) has been their essential even if often unstated assumption. Simplicity is not the sole motive for assuming axial symmetry. The orbit of any spacecraft imposes an inevitable latitude–longitude correlation upon the observations, discussed by Vasyliunas and Dessler [1981] and illustrated in Figure 11.1, as a result of which the available observations, either of the plasma or of the magnetic field, are seriously incomplete in longitudinal coverage at any fixed magnetic latitude and do not provide an adequate basis for a fully longitude-dependent model.

Another assumption widely invoked in constructing theoretical and applying empirical models is that the plasma pressure is isotropic, $P_\perp = P_\parallel = P$. Again, the motive is in part simplicity and in part lack of any clear guidance in the available limited observations toward possible alternatives. An exception are models that assume the plasma in the magnetosphere to be predominantly of ionospheric origin, in which case one expects $P_\parallel \simeq \rho \Omega_J^2 r^2 >> P_\perp$ [e.g., Carbary and Hill, 1978]; however, such models are now of little interest inasmuch as it is well established that the major source of plasma in the Jovian magnetosphere is the Io torus and not the ionosphere (see Chapts. 2, 3, and 10).

1. Theoretical models

The geometrical thinness of the plasma sheet in the Jovian magnetosphere, which is an observationally established property (see Chap. 3) as well as a theoretically expected consequence of the equatorially confined Io source [Hill and Michel, 1976; Siscoe, 1977], permits the construction of a model to be carried out in two steps. First, the large-scale structure of the magnetic field can be calculated from the integrated tangential stress balance Equation (11.19), which with the usual assumption of centripetal acceleration and the idealization of the system as axially symmetric (hence with the current sheet in the common magnetic-rotational equator) may be written in the form

$$-\sigma\omega^2 r = B_z j_\phi' \tag{11.56}$$

where j_ϕ' is the current in the azimuthal direction per unit radial length and r is the cylindrical radial coordinate with respect to the rotation axis. (The pressure terms have been dropped, as discussed in Sec. 11.2.2.) The quantity $\sigma/B_z \equiv \eta$ represents, as pointed out already, the plasma content of a flux tube per unit magnetic flux. Specifying $\eta\omega^2$ as a function of r suffices to determine j_ϕ' everywhere, and the magnetic field can then be calculated by treating the current sheet thickness as infinitesimal and applying standard boundary value methods [e.g., Jackson, 1962, especially his Sec. 5.5 and Problem 5.4]. As the second step, the thickness of the current sheet and the properties of plasma within it can be calculated from the normal component of the momentum equation. The calculation is particularly simple when pressure balance holds: the plasma pressure at the center of the current sheet then is given by

$$P = B_r^2/2\mu_0 \tag{11.57}$$

(where $B_r \approx B_\rho^*$ is the field just outside the sheet), and the general order-of-magnitude relation $\sigma \approx \rho h$ may be written as

$$\rho h \omega^2 = B_z [\sigma\omega^2/B_z] \tag{11.58}$$

giving two equations whose RH sides contain only quantities already available from the first step, either as its input ($\sigma\omega^2/B_z$) or as its result (B_r, B_z). Evidently, from Equations (11.58) and (11.59) the density and the thermal speed can be calculated if $\omega^2 h$ is independently known as a function of r, or alternatively $\omega^2 h$ and ρ can be calculated if a pressure-density relation is known (this includes, as an important special case, specifying the thermal speed as a function of r).

In this section we discuss only the first step, models of the large-scale magnetic field derived from the radial distribution of the single quantity $\eta\omega^2$; current sheet thickness and related questions are deferred to Section 11.3.3. Furthermore, the toroidal magnetic field component B_ϕ is relatively small except in the outermost regions of the Jovian magnetosphere and is neglected in most models (it is discussed in Sec. 11.3.4). With the assumption of axial symmetry and neglect of B_ϕ, **B** is most conveniently derived from the vector potential **A** which now has only a ϕ-component $A_\phi(r, z)$. A

representation of the field by the Euler potential functions f, g (see, e.g., Chap. 1, Sec. 1.3) is then given by

$$f = rA_\phi(r,z) \qquad g = \phi \tag{11.59}$$

The curves defined by $rA_\phi(r,z)$ = constant are magnetic field lines on a meridian plane, and the value of $2\pi rA_\phi$ at any point represents the amount of magnetic flux between the magnetic shell surface through that point and the field line, defined by $rA_\phi = 0$, emanating from the poles of the dipole.

A family of models was obtained by Gleeson and Axford [1976], who assumed for j_ϕ' a family of analytic expressions

$$j_\phi'(r) = \eta_n \Omega_J^2 r / [1 + (r/a_n)^2]^{n+(1/2)} \tag{11.60}$$

which allows **B** to be calculated in closed form. Here n is a positive integer, with $n = 1$, 2 being the cases treated in detail, and η_n and a_n are constants (our notation differs from that of Gleeson and Axford). Comparison of (11.60) with (11.56) implies that the flux tube content times ω^2 varies in the models as

$$\eta\omega^2 = \eta_n \Omega_J^2 / [1 + (r/a_n)^2]^{n+(1/2)} \tag{11.61}$$

that is, constant for $r << a_n$ and decreasing as an inverse power of r for $r >> a_n$ (it makes no difference, as far as the large-scale structure of the model field is concerned, whether the decrease at large r is associated with a decrease of η or ω^2 or both). The vector potential is given by

$$A_\phi(r,z) = \frac{Mr}{(r^2+z^2)^{3/2}} + \frac{MK_1}{a_1 r}\left[1 - \frac{Z_1}{(Z_1^2+r^2)^{1/2}}\right] + \frac{MK_2}{3}\frac{r}{(Z_2^2+r^2)^{3/2}} \tag{11.62}$$

where

$$Z_n \equiv |z| + a_n, \qquad K_n \equiv \mu_0 a_n^4 \eta_n \Omega_J^2 / 2M$$

The first term in (11.62) represents the Jovian dipole field with moment M and the terms multiplied by the constants K_1 and K_2 arise from j_ϕ' of Equation (11.60) with $n = 1$ and $n = 2$, respectively. (Note a misprint in the corresponding equation of Gleeson and Axford, their Equation (20): in the numerator a_2^2 should be a_2^3.) The magnetic field component normal to the current sheet, derived from (11.62), is

$$B_z(r, z=0) = -\frac{M}{r^3}\left\{1 - \frac{K_1 r^3}{(a_1^2+r^2)^{3/2}} - \frac{K_2 r^3 (2a_2^2 - r^2)}{3(a_2^2+r^2)^{5/2}}\right\} \tag{11.63}$$

From (11.63) and (11.61) one can at once calculate the variation of $\sigma\omega^2$ with r.

It is convenient to deal with two separate models, $n = 1$ and $n = 2$, obtained by setting K_2 and K_1 to zero in turn. In both models, the magnetic-field-line configuration is stretched out in comparison to a pure dipole, the degree of stretching increasing with increasing value of K. This is graphically illustrated in a series of figures presented by Gleeson and Axford, but it can also be qualitatively deduced from Equation (11.62) by noting that the value of rA_ϕ at any given point is always larger than the dipole value,

implying that the field line through that point emanates from a lower dipole latitude (for an ideal dipole field at a radial distance of 1 R_J, the Euler potential f has the value

$$f = rA_\phi = M\sin^2\theta/R_J \qquad (\text{at } r^2 + z^2 = R_J^2) \tag{11.64}$$

where θ is the colatitude). However, in the case $n = 2$, the stretching-out becomes insignificant at large distances: when $r^2 + z^2 >> a_2^2$, the field line configuration approaches that of a dipole with moment $M[1 + (K_2/3)]$, and $rA_\phi \to 0$ as $r \to \infty$ with the result that the model contains no open field lines — all the field lines emanating from the dipole eventually close across the equatorial plane (unless, of course, departures from the model at large distances are introduced, caused, for example, by magnetotail currents). On the contrary, in the case $n = 1$ the field line configuration remains non-dipolar out to arbitrarily large distances and $rA_\phi \to MK_1/a_1$ as $r \to \infty$ at fixed z; thus, in this model, all field lines emanating poleward of the dipole colatitude defined by

$$\sin^2\theta = K_1 R_J / a_1 \tag{11.65}$$

are truly open and do not cross the equatorial plane at any distance, no matter how large. These open field lines are present for any value of $K_1 > 0$, even though for $K_1 < 1$ the model does not contain any magnetic singular lines, of $\times$ type or other, either at a finite distance or in the limit $r \to \infty$.

As expected from the stretched-out configuration, the normal component B_z given by (11.63) is reduced in magnitude below the dipole value, everywhere for $n = 1$ and out to a distance $r = (2)^{1/2} a_2$ for $n = 2$. Eventually, as K_1 or K_2 is increased to a critical value, B_z is reduced to zero at some point, indicating the incipient appearance of magnetic singular lines. For $n = 1$, the critical value of K_1 is $K_{1c} = 1$ and the singular line appears at infinity; if $K_1 > 1$, a magnetic $\times$ line is found at a finite distance. For $n = 2$, $K_{2c} = 3/2\,(5/2)^{5/2} \approx 14.8$ and the singular line appears at $r_c = a_2\,(2/3)^{1/2}$; for $K_2 > K_{2c}$, it splits into an $\times$ – $\bigcirc$ line pair with associated closed loops of magnetic field lines. (Note: Gleeson and Axford give incorrect numerical expressions for K_{2c} and r_c, as well as for rA_ϕ at r_c which should be $(3/2)^{5/2}\, M/a_2$.) When the critical value of K is exceeded, B_z given by the model has a reversed sign over a portion of the current sheet, but this is unphysical because Equation (11.56) together with (11.60) then implies a negative mass density σ. Hence follows the important conclusion that, within the Gleeson–Axford family of models, corotating plasma can exist in stress balance only if $K \le K_c$, which is effectively a restriction on the distance of corotation for a given level of flux tube content, as can be seen by using the definition of K_n to write the restriction in the form

$$a_n^4 \le 2K_c\, M/\mu_0 \eta_n \Omega_J^2 \tag{11.66}$$

The distance $r \approx a_n$ represents in a qualitative sense the limit of corotating plasma, because for $r >> a_n$ we have $\eta_n\omega^2 << \eta_n\Omega_J^2$, that is, either the plasma moves much more slowly than corotation or else there is much less of it (or both). The constant η_n may be equated to the flux tube content at the location of the plasma source, that is, $r = r_s = 6\ R_J$ for an Io source, provided $a_n >> r_s$:

$$\eta_n = \eta_s \equiv \rho_s h_s / B_s \tag{11.67}$$

where ρ_s is the plasma mass density and h_s the plasma sheet thickness at the source location (averaged over all longitudes because the model has axial symmetry). By writing $B_s = M/r_s^3$, $M = B_J R_J^3$, using (11.67) and expressing all distances in units of R_J we may cast (11.66) into a more familiar form

$$\left(\frac{a_n}{R_J}\right)^4 \leq \frac{2K_c B_J^2}{\mu_0 \rho_s h_s \Omega_J^2 R_s L_s^3} \tag{11.68}$$

where $L_s \equiv r_s/R_J$.

The model of Hill and Carbary [1978] makes the assumption that rigid corotation and constancy of flux tube content are maintained throughout the closed field line region of the magnetosphere; thus $\eta\omega^2 = \eta_s \Omega_J^2$ as long as $B_z > 0$, out to a distance $r = r_0$ to be determined, and j_ϕ' is given by

$$j_\phi'(r) = \eta_s \Omega_J^2 r \qquad r \leq r_0 \tag{11.69}$$

For $r > r_0$ the plasma can no longer be corotating in stress balance and may be presumed instead to form a planetary/magnetospheric wind as discussed in Section 11.4.3, but for the construction of the model it suffices to assume merely that

$$B_z(r, z = 0) \qquad r \geq r_0 \tag{11.70}$$

Conditions (11.69) and (11.70) together with continuity of j_ϕ' across $r = r_0$ and a dipole at the origin define a boundary value problem with a unique solution (including determination of the value of r_0) which must be obtained numerically. Hill and Carbary found that condition (11.70) could be satisfied to an adequate accuracy by setting

$$j_\phi'(r) = \eta_s \Omega_J^2 r_0 [1.5 (r_0/r)^2 - 0.5 (r_0/r)^3] \qquad r \geq r_0 \tag{11.71}$$

[note that j_ϕ' here is *not* connected with $\eta\omega^2$ by Equation (11.56)]; with j_ϕ' thus specified everywhere, its contribution to **B** can be calculated by numerical integration and expressed as a function of r/r_0 multiplied by the scale factor $\eta_s \Omega_J^2 r_0$. In particular, the part of $B_z(r=r_0, z=0)$ contributed by the current sheet alone, which must be equal and opposite to the dipole field to give $B_z = 0$, may be written as equal to the quantity $B_r/\alpha = \mu_0 \eta_s \Omega_J^2 r_0/2\alpha$, where $\alpha \approx 2$ is a constant given by the numerical calculation; thus r_0 is obtained by setting

$$\mu_0 \eta_s \Omega_J^2 r_0/2\alpha = M/r_0^3 \tag{11.72}$$

which yields

$$r_0^4 = 2\alpha M/\mu_0 \eta_s \Omega_J^2 \tag{11.73}$$

or equivalently

$$\left(\frac{r_0}{R_J}\right)^4 = \frac{2\alpha B_J^2}{\mu_0 \rho_s h_s \Omega_J^2 R_J L_s^3} \tag{11.74}$$

identical to the equalities in (11.66) or (11.68) except for the replacement of K_c by α. The limiting colatitude of open field lines is found to be

$$\sin^2\theta = 1.2\, R_J/r_0 \tag{11.75}$$

to be compared with the corresponding result (11.65) for the $n = 1$ Gleeson–Axford model.

Evidently the model of Hill and Carbary has several points of similarity with the Gleeson–Axford models, particularly with their $n = 1$ case (the $n = 2$ case is of relatively little interest because it has no open field lines). The most highly stretched Gleeson–Axford model has $K_1 = K_c = 1$; therefore the ratio $r_0/a_1 = 2^{1/4} \approx 1.2$, which leads to the remarkable result that the amount of open flux in that model is the same as

in that of Hill and Carbary. Both models have the same asymptotic form $j_\phi' \sim r^{-2}$ as $r \to \infty$; the total current diverges logarithmically if integrated to infinity (contrary to the impression given in the paper of Gleeson and Axford) but all field and plasma quantities remain finite everywhere. The main difference is that Hill and Carbary maintain full corotation and source-imposed flux tube plasma content out to a limiting distance r_0 beyond which stress balance breaks down altogether as field lines no longer cross the equator, whereas Gleeson and Axford maintain stress balance and field line closure at all distances (although a significant amount of magnetic flux remains unclosed even as $r \to \infty$) but allow the flux tube plasma content and/or degree of corotation to fall off gradually at and beyond distances comparable with r_0. In some ways, the Gleeson–Axford model resembles a smoothed-out version of the Hill–Carbary model. A comparison of the two and of other models is presented later in Section 11.3.2.

Vickers [1978] attempted to extend the Gleeson-Axford models by including the effects of tangential pressure gradients. However, these effects are of the same order of magnitude as those due to $\partial B_z/\partial z \neq 0$ within the current sheet, as discussed in Section 11.2.2, and it is shown in Appendix A that this inconsistency invalidates his model. Sozzou [1978] developed a similarity model of a specialized mathematical form with singularities at the origin, which illustrates some effects of rotation and pressure gradients.

2. Empirical models and their implications

Several quantitative models of the magnetic field in the Jovian magnetosphere have been constructed on the basis of empirical fits to some subset of the available in situ magnetic field observations; the reader is referred to Chapter 1, Section 1.3 for a detailed review. Stress balance plays no direct role in the construction of such a model but it does impose significant constraints on the plasma properties if these are to be compatible with the model; in some cases the plasma properties required for compatibility may be physically unreasonable, indicating that some revision of the model is called for. The source of the constraints is the momentum Equation (11.1): with the magnetic field $\mathbf{B}(\mathbf{r})$ given by the model and $\mathbf{j}(\mathbf{r})$ obtained from $\nabla \times \mathbf{B}$, the RH side $\mathbf{j} \times \mathbf{B}$ of (11.1) is a known function of space, and the spatial variation of pressure and density must be such as to yield the same function for the LH side. In the particular case of isotropic pressure and axially symmetric configuration with corotational flow, Equation (11.1) suffices to determine $\rho(r, z)$ and $P(r, z)$, as pointed out by Goldstein [1977].

Written out explicitly in cylindrical coordinates, with the assumption of isotropic pressure and azimuthal flow, Equation (11.1) becomes

$$(\partial P/\partial z)_r = (\mathbf{j} \times \mathbf{B}) \cdot \hat{\mathbf{z}} \tag{11.76}$$

$$-\rho\omega^2 r + (\partial P/\partial r)_z = (\mathbf{j} \times \mathbf{B}) \cdot \hat{\mathbf{r}} \tag{11.77}$$

where the fact that P is a function of r and z is explicitly indicated by showing as subscripts the variables held constant during partial differentiation (it will soon prove useful to introduce another set of variables). With $\mathbf{j} \times \mathbf{B}$ known from a field model, $P(r, z)$ can be calculated by direct integration of (11.76) with a suitable boundary condition, for example, $P \to 0$ as $z \to \infty$; differentiation then yields $(\partial P/\partial r)_z$, and $\rho(r, z)$ can be calculated directly from (11.77). If axial symmetry is assumed, there is no dependence on ϕ so that the spatial variation of P and ρ is known completely. Furthermore, with $\mathbf{j} = j(r, z)\,\hat{\phi}$ and $B_\phi = 0$ the components of $\mathbf{j} \times \mathbf{B}$ assume the simple form

$$(\mathbf{j} \times \mathbf{B}) \cdot \hat{\mathbf{z}} = -jB_r \tag{11.78}$$

$$(\mathbf{j} \times \mathbf{B}) \cdot \hat{\mathbf{r}} = jB_z \tag{11.79}$$

Equations (11.76)–(11.79) provide a complete and readily usable prescription for determining the plasma distribution needed to maintain a given magnetic field configuration in stress balance. They can be cast into a form that is more elegant (although not necessarily more useful for calculation) by introducing the Euler potential or magnetic flux function $f = rA_\phi$ and treating P and ρ as functions of r and f rather than r and z. The partial derivatives are readily transformed by writing

$$dP = (\partial P/\partial r)_z\, dr + (\partial P/\partial z)_r\, dz \tag{11.80}$$

$$df = (\partial f/\partial r)_z\, dr + (\partial f/\partial z)_r\, dz = rB_z\, dr - rB_r\, dz \tag{11.81}$$

and forming the ratios dP/df with $dr = 0$, and so forth; the resulting expressions allow the reduction of (11.76)–(11.79) to

$$(\partial P/\partial f)_r = j/r \tag{11.82}$$

$$(\partial P/\partial r)_f = \rho\omega^2 r \tag{11.83}$$

Equations (11.82)–(11.83) were derived by Goldstein [1977] on the basis of a restrictive assumption that the plasma electron and ion velocity distribution functions are special solutions of the Vlasov equation depending on the two explicitly known constants of motion, energy, and canonical angular momentum about the symmetry axis (whereas the general solution for a time-independent axially symmetric system depends on four constants of motion). The derivation given here makes it apparent that Goldstein's results are more general, presupposing only the momentum equation with isotropic pressure and axial symmetry.

An even simpler form of the equations results if an effective potential U for the acceleration is introduced,

$$U \equiv (1/2)\omega^2 r^2 \tag{11.84}$$

(this form of U presupposes that ω depends at most only on f, that is, ω is constant along a field line, in accordance with Ferraro's isorotation theorem): with P and ρ now treated as functions of U and f, it is readily shown that

$$(\partial P/\partial f)_U = j/r \tag{11.85}$$

$$(\partial P/\partial U)_f = \rho \tag{11.86}$$

It is now also evident that the equations can be generalized to the case when the effective acceleration of the plasma does not have the simple centripetal form, by merely changing U appropriately; for example, if the gravitational term is nonnegligible, (11.84) is replaced by

$$U \equiv (1/2)\omega^2 r^2 - M_J G/(r^2 + z^2)^{1/2} \tag{11.87}$$

In whichever form the equations are used, it is possible to calculate both the plasma mass density and the pressure everywhere, given *any* field model; there are no general restrictions on the model magnetic field other than effective axial symmetry (but also there is no a priori assurance that the calculated ρ and P will be plausible or even physically realizable). A contrasting situation arises when the inertial terms in the momentum equation are negligibly small, as for the terrestrial magnetosphere in models of the symmetric ring current [e.g., Carovillano and Siscoe, 1973; and references therein] and

in two-dimensional models (with a planar rather than cylindrical geometry) of the plasma sheet [e.g., Schindler, 1975, 1979]: in these cases only the pressure distribution can be calculated, no information on the density being obtainable from the magnetic field, and the field model itself is required to satisfy the rather restrictive constraint that j/r (or j, for a planar geometry) must be constant along field lines, a restriction that follows from Equation (11.82) together with the constancy of P along field lines implied by Equation (11.83) when $\rho\omega^2 r$ is negligible. Rotational stresses in the Jovian magnetosphere are thus indispensable if inferences about the plasma distribution are to be drawn from empirical models of the magnetic field, constructed for the most part without imposing any particular constraints.

Empirical models developed to a sufficient extent to enable the derivation of plasma parameters by the method described above include (see Chap. 1 for a detailed description) the model of Goertz et al. [1976] (slightly modified by Jones, Melville, and Blake [1980]), applicable at distances between 20 and 80 R_J in the predawn local time sector, and the model of Connerney, Acuña, and Ness [1981], applicable out to a distance of about 30 R_J at all local times. There is also the model of Barish and Smith [1975], commonly thought to represent the magnetic field in the dayside magnetosphere; however, as shown in Appendix A, this model in its main features differs considerably from what is either observed or theoretically expected.

For the model of Goertz et al., Goldstein [1977] has calculated the implied distribution of plasma mass density and pressure in full detail, using Equations (11.82) and (11.83). An alternative simpler treatment has been presented by Goertz et al. [1979]. For many purposes, the quantities of prime interest are the pressure and mass density at the center of the current sheet, the rest of the spatial distribution being adequately described by the value of current sheet thickness and the statement that P and ρ are negligibly small outside the current sheet. The magnetic field configuration, within the distance range where the model is applicable, is sufficiently taillike so that integration of Equation (11.76) to obtain P leads to a simple pressure balance relation, as in Section 11.2. Hence the plasma pressure at the center is well approximated by the magnetic pressure outside the current sheet or

$$P(r, z = 0) = b_0^2/2\mu_0 D^2 r^{2a+2} \tag{11.88}$$

in terms of the usual parameters of the model: $b_0 = 9 \times 10^3\, nT\, R_J^{2+a}$ (note the units of b_0, which are not properly given either in Goertz et al. [1976] or in Chap. 1), $D = 1\ R_J$, the half thickness of the current sheet, and $a = 0.7$. [Equation (11.88) differs slightly but not significantly from the results of Goertz et al. [1979], because of an ambiguity in the model at large values of $|z|$, discussed in Appendix A.] From Equation (11.77) and the radial derivative of Equation (11.88) one obtains the mass density $\rho(r, z = 0)$ with the result given, to within $O(D^2/r^2)$, by

$$\rho\omega^2 = (b_0 M/\mu_0 D^2 r^{a+5})\,(1 - c_1 r^{1-a}) \tag{11.89}$$

where M is the Jovian dipole moment,

$$c_1 \equiv b_0(aC + a + 1)/M \tag{11.90}$$

and the value of the model parameter C is given as $C = 10$ by Goertz et al. [1976] and $C = 15$ by Jones, Melville, and Blake [1980].

For the model of Connerney, Acuña, and Ness [1981], no estimates of the implied plasma parameters have yet appeared in the literature. They can, however, be calculated fairly easily, owing to the simple form of the azimuthal current density in the model:

$$\mu_0 j_\phi = B_0/r \qquad \text{for } |z| < D,\ r_0 < r < r_1 \qquad (11.91)$$
$$= 0 \qquad \text{elsewhere}$$

where the adopted parameter values are $D = 2.5\ R_J$, $r_0 = 5\ R_J$, $r_1 = 50\ R_J$, and $B_0 = 450\ nT$ or $300\ nT$ if the model is fitted to Voyager 1 or Voyager 2 observations, respectively (see Chap. 1, Sec. 1.3 for a more detailed presentation). The model's intended range of applicability extends deep into the inner magnetosphere where the magnetic field is nearly dipolar and the pressure balance approximation is *not* valid. The pressure must thus be calculated by an explicit integration of Equation (11.76), but with j given by (11.91) and with the model field represented by the analytical approximations given by Connerney, Acuña, and Ness [1981] (reproduced here in Chap. 1, Appendix A) the integration can be carried out in closed form. With the boundary condition $P = 0$ at $z = \pm D$, required by the fact that $\mathbf{j} \times \mathbf{B} = 0$ for $|z| > D$ in the model, the calculated pressure is given by

$$P(r, z) = (MB_0/\mu_0)\{(r^2 + z^2)^{-3/2} - (r^2 + D^2)^{-3/2}\} \qquad (11.92)$$
$$+ (B_0^2/2\mu_0)\{(D^2 - z^2)/r^2 + G_1 + G_2 + (r_0^2/4r^2)G_3\}$$

where

$$2r^2 G_1 \equiv (z + D)[(z + D)^2 + r^2]^{1/2} - (z - D)[z - D)^2 + r^2]^{1/2} \qquad (11.93)$$
$$- 2D[4D^2 + r^2]^{1/2}$$
$$2G_2 \equiv \sinh^{-1}[(z + D)/r] - \sinh^{-1}[(z - D)/r] - \sinh^{-1}[2D/r]$$
$$G_3 \equiv 2D[4D^2 + r^2]^{-1/2} + (z - D)[z - D)^2 + r^2]^{-1/2}$$
$$- (z + D)[(z + D)^2 + r^2]^{-1/2}.$$

Equation (11.92) holds for $r > r_0$, $|z| < D$; the model implies zero pressure for $r < r_0$ and for $|z| > D$, whereas for $r \to r_1$ the model becomes inapplicable and we shall use the model results only out to about $r = 0.6\ r_1 = 30\ R_J$. The terms in the first set of curly brackets in (11.92) arise from the current sheet's interaction with the dipole field alone and the rest from its interaction with its own field; as r increases, the former become negligibly small and the latter approach the expected pressure-balance value

$$P(r, z) \approx (B_0^2/2\mu_0)(D^2 - z^2)/r^2 \qquad (11.94)$$

The plasma mass density profile $\rho(r, z)$ implied by the model, obtained from Equation (11.77) with the radial pressure gradient from (11.92), is given by

$$\rho\omega^2 r^2 = (MB_0/\mu_0)\{3r^2(r^2 + D^2)^{-5/2} - 2(r^2 + z^2)^{-3/2}\} \qquad (11.95)$$
$$- (B_0^2/2\mu_0)\{2(D^2 - z^2)/r^2 + 2D[(z^2 + r^2)^{-1/2} - (z^2 + r_1^2)^{-1/2}]$$
$$+ G_1 + (r_0^2/2r^2)\,G_3\} + r_0 P_0 \delta(r - r_0)$$

where G_1 and G_3 are given by (11.93) and P_0 is the value of $P(r, z)$ given by (11.92) as $r \to r_0^+$. The density is zero for $r < r_0$ and for $|z| > D$. The delta function in density at

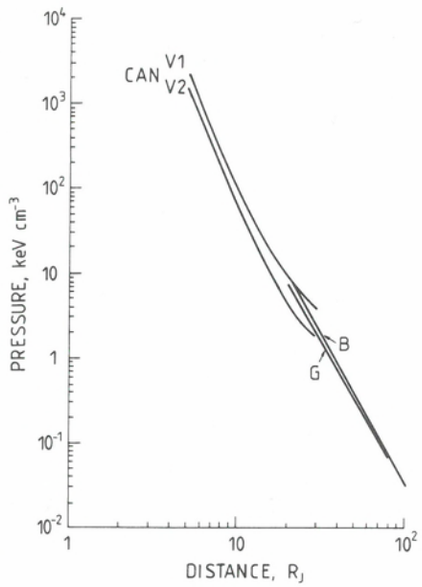

Fig. 11.2. Plasma pressure at the center of the current sheet calculated from the magnetic field model of Connerney, Acuña, and Ness [1981] (CAN) and the magnetic field model of Goertz et al. [1979] (G), and calculated from pressure balance with the observed field by Barbosa et al. [1979] (B).

the inner edge of the current sheet results from the assumed abrupt termination of j; a gradual fall-off over a distance range Δr would lead to a finite density spike of radial width Δr.

Figure 11.2 shows the calculated pressure at the center of the current sheet ($z = 0$) for both the Connerney, Acuña, and Ness model and the Goertz et al. model; in addition, an empirical determination from magnetic field observations and pressure balance published by Barbosa et al. [1979] is shown for comparison. The various curves are in fair agreement with each other, and the general radial profile is smooth and shows no unexpected or questionable features. The numerical values are roughly consistent with the direct observational determinations of the plasma pressure, available (albeit with sizable uncertainties) at distances beyond 10 R_J [Lanzerotti et al., 1980; Krimigis et al., 1981].

The situation with the calculated mass density, shown in Figure 11.3, is far less satisfactory. Three problem areas are at once evident from the figure: (1) negative density in some regions, (2) disagreement between the two models where they overlap, (3) discrepancy, beyond 20 R_J, between the density radial gradient derived from the models and estimated from plasma wave observations [Barbosa et al., 1979].

(1) The mass density implied by either the V 1 or V 2 version of the Connerney, Acuña, and Ness model is negative in the equatorial plane from about 6.2 R_J inward, until the (positive) δ-function spike at 5 R_J. This occurs because the inward-directed radial pressure gradient exceeds the (likewise inward-directed) radial component of the $\mathbf{j} \times \mathbf{B}$ force density, and the requirement of stress balance then forces the centripetal acceleration term $-\rho\omega^2\mathbf{r}$ to be directed outward. In turn, the excessively large pressure is traceable to a too large thickness D. At these close distances, the current sheet interacts primarily with the dipole field (hence, incidentally, any inaccuracies in the analytical approximations to the model field are of no consequence); P at $z = 0$ varies nearly as $B_0 D^2$ [see Eq. (11.92)], one factor D coming from the length of the integration in $\int_0^D dz\, jB_r$ and the other from the z dependence of the dipolar B_r, and the radial component of $\mathbf{j} \times \mathbf{B}$ varies as B_0. According to Connerney, Acuña, and Ness [1981], the quantity $B_0 D$ is well determined by the observations, whereas D is rather uncertain.

Fig. 11.3. Plasma mass density times $(\omega/\Omega_J)^2$ at the center of the current sheet, calculated from the same models as in Figure 11.2; for the magnetic field model of Goertz et al., parameter values given by Goertz et al. [1976] (G) and by Jones, Melville, and Blake [1980] (JMB) were used. The mass density values inferred from Barbosa et al. [1979] (B) assume $\omega = \Omega_J$ and mean atomic mass number either $A = 1$ or $A = 16$.

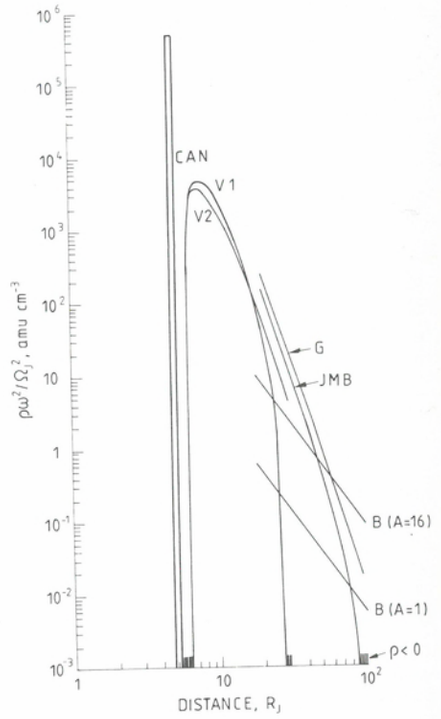

Fig. 11.4. Plasma mass density times $(\omega/\Omega_J)^2$ and pressure at the center of the current sheet at $r = 6R_J$, calculated from the V 1 model of Connerney, Acuña, and Ness [1981], as a function of assumed current sheet thickness D (for a fixed value of B_0D).

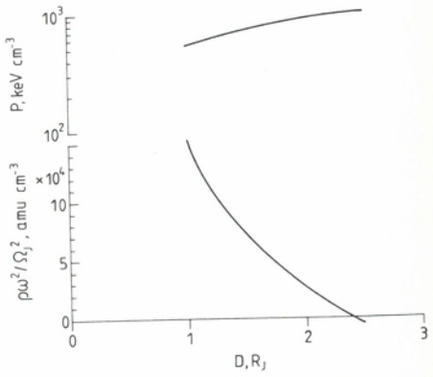

Hence, with fixed B_0D, $\partial P/\partial r \sim D$ and $(\mathbf{j} \times \mathbf{B}) \cdot \hat{\mathbf{r}} \sim 1/D$, and a negative mass density is obtained if D is chosen too large. This is illustrated in Figure 11.4, where the equatorial mass density and pressure at $r = 6\ R_J$ are calculated from the Connerney, Acuña, and Ness model for various values of D. As expected, ρ falls sharply with increasing D and becomes negative for $D \geq 2.4\ R_J$; to match the density of $\sim 3 \times 10^4$ amu/cm^3 at $r = 6\ R_J$ inferred from plasma observations (see Chap. 3, Figs. 3.8, 3.11, 3.12), one needs $D \approx 1.9\ R_J$.

It is thus possible to eliminate the inner negative density region (and with it the sharp density decrease at 7–8 R_J, produced by the same cause) merely by choosing a smaller thickness for the model current sheet; the associated reduction of the pressure, also shown in Figure 11.4, is not very large and does not significantly affect the pressure

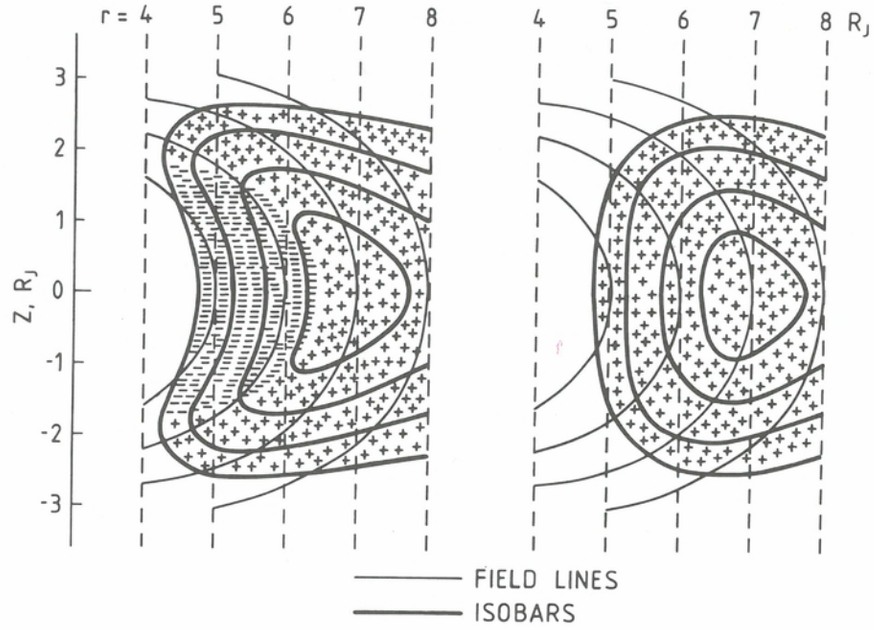

Fig. 11.5. Qualitative configuration of constant pressure curves and positive and negative current density regions near the inner edge of the current sheet, deduced from Equation (11.85) (sign of j_ϕ depends on whether the pressure decreases or increases along a centrifugal equipotential) and Equation (11.86) (positive density requires pressure to decrease with decreasing centrifugal potential along a field line). Left: isobars at the inner edge nearly aligned with field lines, giving rise to positive and negative current regions. Right: current everywhere positive, requiring isobars to be curved away from the centrifugal equipotentials.

profile in Figure 11.2. However, the model then still contains an unphysical feature, the infinite density spike at 4–5 R_J; the infinity can of course be removed by assigning a finite radial width Δr to the inner edge of the current sheet, but even with $\Delta r = 0.5\ R_J$, assumed in Figure 11.3 (and close to the width of observed density features, e.g., Fig. 3.7), the maximum value of ρ exceeds by an order of magnitude anything that has been observed. This large (positive) mass density enhancement is required in order for the centripetal acceleration to balance the *outward* radial pressure gradient that exists at the inner edge of the current sheet, it being assumed in the model that $\mathbf{j} \times \mathbf{B}$ remains inwardly pointing throughout. In reality, however, if this huge density enhancement is not present, the system will achieve stress balance by developing a reversed current at the sheet's inner edge, so that $\mathbf{j} \times \mathbf{B}$ there points outward (a possibility not considered when the model was constructed and fitted to observations). The expected qualitative configuration, easily deduced with the help of Equations (11.85) and (11.86), is sketched in Figure 11.5: if the isobars in the meridian plane are curved in the same sense as the magnetic field lines, there is a crescent-shaped region of reversed current at the inner edge where the pressure decreases with decreasing radius. (In order for j to have the same sign everywhere, the isobars in the region of decreasing pressure must curve in the opposite sense from the field lines, away from the rotation axis.) What effect the inclusion of a current sheet inner edge of finite width and with

reversed current would have on the model, in particular on estimates of the sheet thickness and calculation of the implied mass density, is at present unknown. Clearly, the Connerney–Acuña–Ness model at distances less than about 8 R_J is in some need of revision.

Other regions of negative mass density occur beyond about 27 R_J (near the end of the model's range of applicability) for the Voyager 1 version only of the Connerney–Acuña–Ness model and beyond 87.5 R_J for the model of Goertz et al. with the parameters of Jones, Melville, and Blake ($C = 15$) only. The physical reason for the negative density is the same as before; however, at these distances pressure balance holds and the radial pressure gradient is fairly reliably determined by the magnetic field observations, hence the fault must lie in the estimate of jB_z. Either j in the models is too small (presumably because of a too large assigned current sheet thickness, again) or B_z has been underestimated; unlike the case of the inner region where B_z is reliably given by the dipole field, B_z here is sensitive to the model assumptions. For the model of Goertz et al., the occurrence of negative ρ is analytically predicted from Equation (11.89) for distances $r > r_d$ defined by

$$r_d^{1-a} = M/b_0(aC + a + 1) \tag{11.96}$$

For $C = 15$, $r_d = 87.5\ R_J$ as previously stated; for $C = 10$, $r_d = 270\ R_J$ lies outside the model's range of applicability. The distance r_d is less than the distance r_{nl} of the neutral line where B_z changes sign, given by

$$r_{nl}^{1-a} = M/b_0\, aC \tag{11.97}$$

with values 144 R_J and 558 R_J for $C = 15$ and 10, respectively, in both cases outside the model's range of applicability. Note that the mass density implied by the empirical models can be negative even in regions where B_z is not reversed in sign compared to the dipole field; in such a case, $\mathbf{j} \times \mathbf{B}$ still has the appropriate inward orientation and is merely too small in magnitude to balance the radial pressure gradient. Only for theoretical models (such as those of Gleeson and Axford) that assume negligible current sheet thickness is the appearance of negative mass density tantamount to a reversal of B_z.

(2) In the distance range 20–30 R_J both models should be applicable and (with the exception of the V 1 model of Connerney, Acuña, and Ness) neither contains evident unphysical features, yet the calculated mass density values for the Goertz et al. model are systematically higher than for the Connerney–Acuña–Ness V 2 model, by a factor of about 4.5 (if $C = 10$) or 2.7 (if $C = 15$). The current sheet thickness in the Goertz et al. model, however, is smaller by a factor of 2.5, so that the mass density integrated across the thickness has rather comparable values in the two models. This suggests that the density difference is related to the as yet unresolved discrepancy in the current sheet thickness. Comparison of Figure 11.3 with the observed equatorial values shown in Figures 3.12 and 3.14 tends to favor the Connerney–Acuña–Ness model.

(3) At larger distances, the mass density implied by the model of Goertz et al. may be compared with the density radial profile between 20 and 100 R_J reported by Barbosa et al. [1979]. This profile, derived from plasma wave observations, refers to the electron concentration and must be multiplied by the average ion mass-to-charge ratio A/Z to obtain the mass density (Fig. 11.3 shows the profile for $A/Z = 1$ and for $A/Z = 16$); furthermore, it is of course independent of any assumptions about corotation, whereas the model predicts not ρ but $\rho(\omega/\Omega_J)^2$. It is at once apparent that the two differ markedly in the radial dependence of the density: n_e inferred from observations decreases with increasing distance as $1/r^{2.75}$, and $\rho(\omega/\Omega_J)^2$ decreases somewhat faster than $1/r^{5.7}$ [see Eq. (11.89)] — a discrepancy by a factor r^3. In principle, there are several possible explanations. A change in the ion composition from mostly sulfur and oxygen at close distances to mostly hydrogen farther out would make ρ decrease faster than n_e, but a change in A/Z by a factor of about $(100\ R_J/20\ R_J)^3 = 125$ is surely out of the question. If the current sheet thickness actually decreases with increasing distance, the correct mass density will decrease more slowly than that inferred from the model with assumed constant thickness, but the required variation of the thickness is $\sim 1/r^3$, that is, a decrease from, say, 4 R_J at $r = 20\ R_J$ to 0.03 R_J at $r = 100\ R_J$, which seems rather farfetched and implausible. The most likely explanation is that $(\omega/\Omega_J)^2$ decreases with increasing distance; there is both theoretical and observational evidence for such a partial corotation of magnetospheric plasma, discussed in Section 11.4.4. Quantitatively, to reconcile the two profiles one needs to assume that, approximately, $\omega \sim 1/r^{3/2}$ or equivalently $V_\phi \sim 1/r^{1/2}$.

Having calculated P and $\rho(\omega/\Omega_J)^2$ implied by the various models, one may form their ratio and obtain a temperature per unit mass divided by $(\omega/\Omega_J)^2$, shown in Figure 11.6 ($P/\rho \equiv kT/A \equiv w^2$ where w is the thermal speed); note that, with A taken to be the average mass of the *ions*, kT is the *sum* of electron and ion temperatures, and the average ion kinetic energy of thermal motion is equal to $(3/2)Aw^2/(1 + T_e/T_i)$. The differences between the temperatures implied by the various models reflect, of course, merely the differences in the densities (Fig. 11.3) which have already been discussed. The minimum at $r \sim 10\ R_J$ for the model of Connerney, Acuña, and Ness is probably an artifact of too low density estimates as the negative density region is approached. The model of Goertz et al. predicts, if $\omega = \Omega_J$ is assumed, a pronounced increase of temperature with increasing radius, as noted by Goldstein [1977] and Goertz et al. [1979]; if, on the other hand, $\omega \sim 1/r^{3/2}$ as just discussed, the temperature decreases nearly as $1/r$ [see also Barbosa et al., 1979]. If the model quantities in Figure 11.6 are divided by twice the corotational energy per unit mass, $\Omega_J^2 r^2$ (also shown as a line in the figure), the result is $(w/V_\phi)^2$, the square of the ratio of the thermal speed to the actual (not the rigidly corotating) azimuthal speed, whose value is given independently of any assumptions about A or ω/Ω_J; according to both models, this ratio lies below unity, although

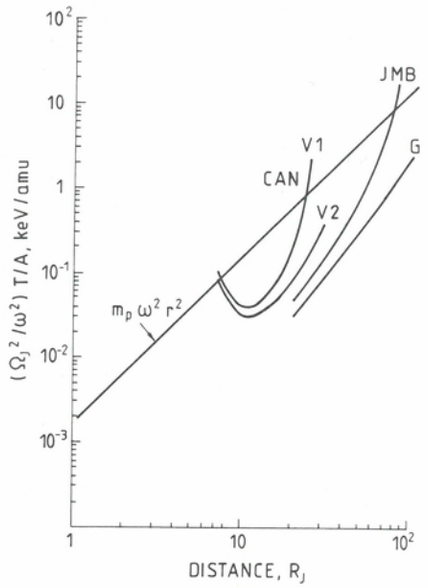

Fig. 11.6. Plasma temperature per unit mass times $(\Omega_J/\omega)^2$ at the center of the current sheet calculated from various magnetic field models (same nomenclature as in Fig. 11.3). The straight line corresponds to thermal speed equal to the actual azimuthal speed (for any value of A and Ω_J/ω).

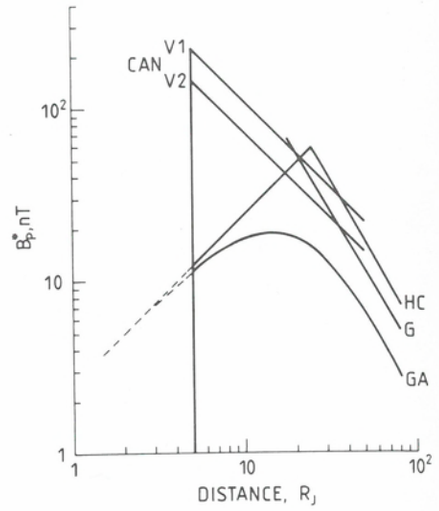

Fig. 11.7. Current density integrated across the half-thickness of the current sheet and expressed as an equivalent planar magnetic field, for various theoretical models [Gleeson and Axford, 1976, GA; Hill and Carbary, 1978, HC] and empirical models (same nomenclature as in Fig. 11.2).

not by more than a factor of 10, nearly everywhere (the few exceptions occur close to regions of apparent negative density and are therefore suspect).

Finally, a comparison between the empirical models and the theoretical models discussed in Section 11.3.1 is presented in Figures 11.7 and 11.8. Suitable quantities for the comparison are the integrated current density, expressed as the equivalent planar field B_p^* (Fig. 11.7), which measures the tangential magnetic stress per unit flux, and the normal component of the magnetic field at the current sheet B_z (Fig. 11.8), which describes the magnetic flux crossing the current sheet; both of these quantities can be specified without reference to the sheet thickness, which is neglected in the theoretical models and and uncertain in the empirical ones. To fix the numerical values of the theoretical model parameters, we write the plasma content per unit magnetic flux η_s at the source distance $r_s = 6\ R_J$ as

$$\eta_s = \rho_s h_s / B_s = [\mu_0 \rho_s / B_s^2]\,(M/r_s^3)\, h_s/\mu_0 \tag{11.98}$$

and take $h_s = 1\ R_J$ and (from Fig. 3.11) $B_s/(\mu_0 \rho_s)^{1/2} = 250$ km/s. The Hill–Carbary model is then completely specified; the distance to the singular line is $r_0 = 24.2\ R_J$. The Gleeson–Axford model has an additional parameter K_1 (or equivalently the distance a_1) which has been set to the critical value $K_1 = 1$ (corresponding, with the above value of η_s, to $a_1 = 20.4\ R_J$) at which a singular line first appears at infinity; even if the singular line is allowed to move in to, say, 120 R_J, the model remains practically unchanged, with $K_1 = 1.044$ and $a_1 = 20.6\ R_J$.

The most striking feature of Figure 11.7 is the discrepancy, reaching an order of magnitude, between the empirical and the theoretical models in the inner magnetosphere. At distances from 6 to 8 R_J, the theoretical calculation of the integrated current implied by the centripetal acceleration of the observed plasma is subject to relatively few uncertainties. The much larger current deduced from the empirical models indicates, therefore, that the dominant tangential stress in the inner magnetosphere arises from plasma pressure gradients rather than rotational stresses. (The importance of plasma pressure here has been argued also on direct observational grounds, e.g., Krimigis et al. [1981] and Chap. 4.) In the outer magnetosphere, beyond 20 R_J, the models exhibit considerably more similarity in the integrated current and it is at least

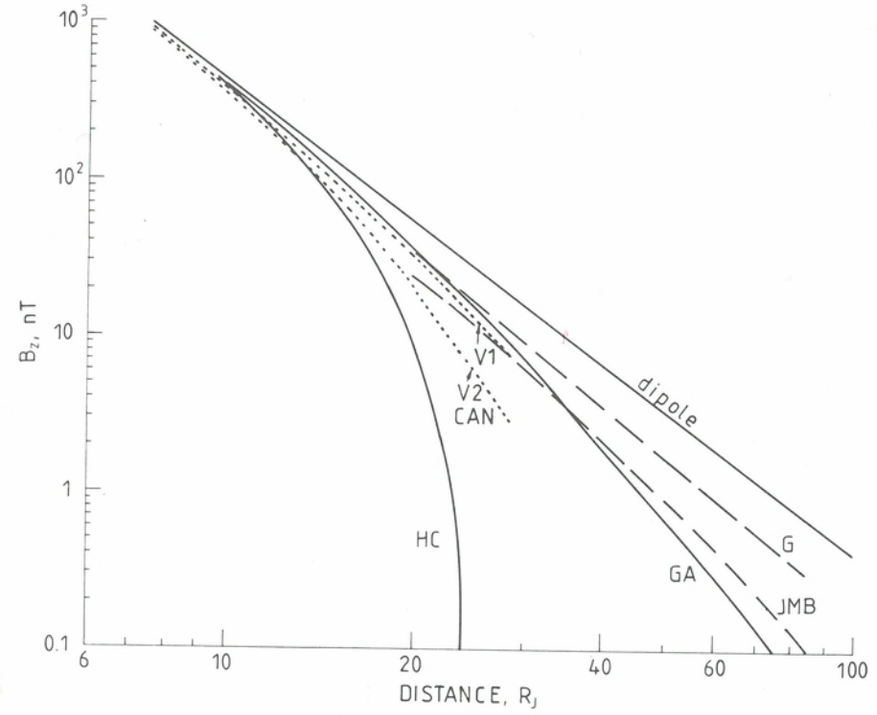

Fig. 11.8. Magnetic field component normal to the current sheet, for various theoretical and empirical models (same nomenclature as in Fig. 11.3 and 11.7).

plausible that rotational effects constitute a major part of the total stress. As to the normal component shown in Figure 11.8, there is a great diversity of model representations, with few common trends other than the fact that B_z is everywhere reduced below its dipole value. Evidently, the distribution of magnetic flux (and hence of the plasma content per unit flux) in the outer Jovian magnetosphere is still poorly understood, from either a theoretical or an empirical viewpoint.

3. Radial variation of current-sheet thickness

To determine the thickness of the current sheet or of the associated plasma sheet from direct observations of the magnetic field or of particle intensities presents a difficult problem because the observational data are functions of time along the spacecraft trajectory and a specific model of current-sheet shape and motion is needed to relate them to distance from the center of the sheet. As an example of how model-dependent such determinations are, Thomsen and Goertz [1981a] show that a particular set of particle observations yields a plasma sheet thickness that is either nearly independent of radial distance or increases in proportion to it, according to whether one assumes a bent-disc model or a magnetic-anomaly-based model for the shape of the sheet [see Vasyliunas and Dessler, 1981; Chap 10, Section 7). Any theoretical constraints on the thickness are therefore of considerable interest. Stress-balance arguments leading to an estimate of the current-sheet thickness have been discussed in Section 11.2.2; for the outer

magnetosphere (the region of prime interest for this purpose) the basic result is given in Equation (11.40) which, specialized to the case of isotropic pressure, can be rewritten as

$$h = [(2r/\nu)\,|B_z/B_p^*|]\,[1/(\mu + 1)] \tag{11.99}$$

where ν is given in (11.26) and

$$\mu \equiv V_\phi^2/\nu w^2 = \omega^2 r^2/\nu w^2 \tag{11.100}$$

Equation (11.99) for h is conveniently viewed as a product of two factors. The quantity within the first set of brackets depends only on the magnetic field, specifically on the integrated current and the normal component as functions of r; the quantity within the second set of brackets depends on the ratio of azimuthal flow speed to thermal speed and does not explicitly depend on the magnetic field (except insofar as the field fixes ν through pressure balance). The first quantity also represents the maximum thickness h_{max}, reached in the limit $\mu \to 0$, that is, azimuthal flow speed negligible compared to thermal speed.

As discussed already in Section 11.3.1, calculation of h by this method is a logical second step in the case of theoretical models of the field, which supply the first factor and then require further assumptions on the plasma temperature and flow for the second. In the case of empirical models, on the contrary, it must be clearly understood that this approach is not complementary but alternative to the one described in Section 11.3.2. To calculate the plasma parameters implied by an empirical magnetic field model, the thickness must have already been specified as part of the model; if the calculated plasma parameters are inserted along with the model field into Equation (11.99), one obtains no new information but merely recovers the previously assumed model thickness. It is possible, on the other hand, to use only the magnetic field from an empirical model and to evaluate μ on the basis of some other assumptions about the plasma. One obtains then an independent model for h as a function of distance, which in general will not be consistent with the thickness parameters of the magnetic field model.

Two calculations of the current sheet thickness by means of the above semiempirical method have appeared in the literature, Goertz [1976b] and Liu [1982]. Both make use of the empirical field model of Goertz et al., and the difference between the approaches of the two illustrate some of the ambiguities of the method. According to its usual parametrization, the model of Goertz et al. has

$$B_p^* = b_0/Dr^{1+a},\ B_z = (M/r^3) - (ab_0\,C/r^{2+a}) \tag{11.101}$$

hence, with $\nu = 2(1 + a)$ implied by pressure balance,

$$\begin{aligned} h &= [aCD/(1 + a)\,(1 + \mu)]\,[(M/ab_0\,Cr^{1-a}) - 1] \\ &= [aCD/(1 + a)\,(1 + \mu)]\,[(r_{nl}/r)^{1-a} - 1] \end{aligned} \tag{11.102}$$

where r_{nl} is the distance to the neutral line given by Equation (11.97). Liu [1982] assumed that the power-law dependences $B_r \sim 1/r^{1+a}$ and $B_z - B_{dipole} \sim 1/r^{2+a}$ are the primary feature of the Goertz et al. model, to be preserved in the calculation, which demands that D in Equations (11.101) and (11.102) be considered a constant. Specification of h as a function of r is then completed by inserting into (11.102) the numerical values of the constants b_0, a, C, D, M and obtaining μ by an independent argument (to be discussed later).

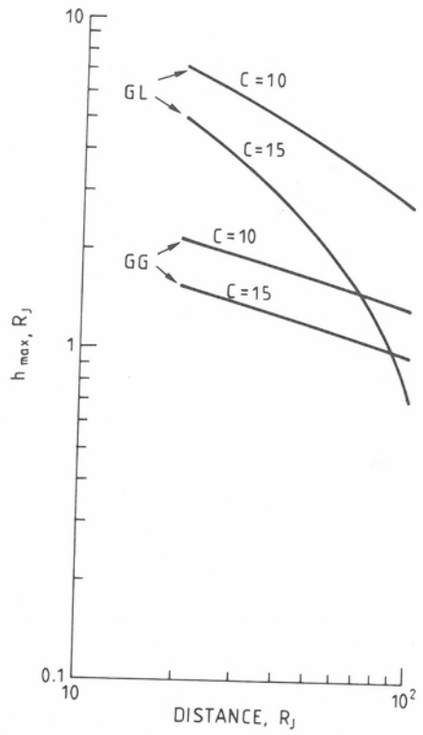

Fig. 11.9. Maximum thickness of the current sheet, reached in the limit $w^2 >> V_\phi^2$, calculated from the model of Goertz et al. [1976] as interpreted by Goertz [1976b] (GG) and by Liu [1982] (GL).

Goertz [1976b] assumed, on the other hand, that the model parameter D is to be identified with the actual and variable current sheet thickness h; to preserve the observationally well-established dependence $B_r \sim 1/r^{1+a}$, he parameterized the model as

$$B_p^* = b_0'/r^{1+a},\ B_z = (M/r^3) - (ab_0'\,CD/r^{2+a}) \tag{11.103}$$

where $b_0' \equiv b_0/D = 9 \times 10^3\,nT\,R_J^{1+a}$ (note the units for b_0') is to be kept constant as D varies. (Note: in the paper of Goertz [1976*b*], b_0' is designated b_0 and given the units of Gauss, or $10^5\,nT$; other than the formulas, there is no hint anywhere that the model parametrization differs from that of Goertz et al. [1976].) Instead of (11.102) one then has

$$h = [aC/(1 + a)\,(1 + \mu)]\,[(M/ab_0'\,Cr^{1-a}) - D] \tag{11.104}$$

and it is assumed that $D = h$, whereupon the equation can be solved for h:

$$h = M/\{b_0'\,r^{1-a}\,[aC + (1 + a)\,(1 + \mu)]\} \tag{11.105}$$

With this value for $h = D$, $B_z - B_{dipole}$ no longer varies as $1/r^{2+a}$; combining (11.105) with (11.103) we have

$$B_z = (M/r^3)\,\{1 - aC/[aC + (1 + a)\,(1 + \mu)]\} \tag{11.106}$$

that is, B_z is now simply the dipole field reduced by a constant factor. In this version of the Goertz et al. model $B_z \neq 0$ at all finite distances; there is no neutral line and hence no last closed field line.

The maximum thickness h_{max} predicted by both models in the hot plasma limit $\mu \to 0$ is shown in Figure 11.9. Equation (11.102) predicts an h_{max} that is relatively large at